INSTITUTE OF PHYSICS PUBLISHING PLASMA PHYSICS AND CONTROLLED FUSION

Plasma Phys. Control. Fusion **46** (2004) 1877–1889 PII: S0741-3335(04)76931-6

Density peaking in low collisionality ELMy H-mode in JET

M Valovič[1], R Budny[2], L Garzotti[1], X Garbet[3], A A Korotkov[1], J Rapp[4], R Neu[5], O Sauter[6], P deVries[7], B Alper[1], M Beurskens[7], J Brzozowski[8], D McDonald[1], H Leggate[1], C Giroud[1], V Parail[1], I Voitsekhovitch[1] and JET EFDA contributors[9]

[1] EURATOM/UKAEA Fusion Association, Culham Science Centre, Abingdon, Oxfordshire OX14 3DB, UK
[2] PPPL Princeton, University NJ, USA
[3] Association EURATOM-CEA, CEA-Cadarache, 13108 Saint Paul Lez Durance, France
[4] Institut für Plasmaphysik, Forschungszentrum Jülich GmbH, EURATOM Association, D-52425 Jülich, Germany[10]
[5] Max-Planck-Institut für Plasmaphysik, IPP-EURATOM Assoziation, Boltzmann-Str. 2, D-85748 Garching
[6] CRPP Lausanne Centre de Recherches en Physique des Plasmas, Association EURATOM-Switzerland, EPFL 101, Switzerland
[7] EFDA Association EURATOM-FOM Institute for Plasma Physics, Rijnhuizen, PO Box 1207, 3430 BE Nieuwegein, Netherlands
[8] EFDA KTH Royal Institute of Technology, Stockholm, Sweden

Received 1 March 2004, in final form 3 September 2004
Published 16 November 2004
Online at stacks.iop.org/PPCF/46/1877
doi:10.1088/0741-3335/46/12/006

Abstract

Low collisionality, low particle source, ELMy H-modes (type-III) with sawteeth are produced in JET in order to address the question of density profile evolution in the reference $q_{95} = 3$ ITER scenario. The paper focuses on particle transport in the core zone around the mid-radius. The pedestal region including ELMs and the region affected by sawteeth are not considered. By replacing a significant part of the neutral beam heating by RF power the beam particle flux at mid-radius has been reduced to $\Gamma_{\mathrm{Beam}}/n_{\mathrm{e}} = 0.07\,\mathrm{m\,s^{-1}}$. The additional flux due to wall neutrals is estimated as $\Gamma_{\mathrm{Wall}}/n_{\mathrm{e}} \leqslant 0.12\,\mathrm{m\,s^{-1}}$. Density profiles are found to be modestly peaked under these conditions with a relative density difference of $\Delta n/\langle n\rangle = 0.23$ across the zone not affected by sawteeth and ELMs. In a region around the mid-radius the ratio of effective particle diffusivity to electron thermal diffusivity is found to be $D_{\mathrm{e,eff}}/\chi_{\mathrm{e}} \approx 0.2$, which might indicate an anomalous pinch provided the particle diffusivity D_{e} is sufficiently large. The measured values of $D_{\mathrm{e,eff}}/\chi_{\mathrm{e}}$ are at the lower end of the range used in ITER models.

[9] See annex of Paméla J *et al* 2003 *Fusion Energy 2002: Proc. 19th Int. Conf. (Lyon, 2002)* (Vienna: IAEA).
[10] Partner in the Trilateral Euregio Cluster.

1. Introduction

The question of whether density profiles in future burning plasmas such as in ITER will be flat or peaked has recently attracted considerable attention. The reason for this is that the shape of the density profile has consequences for the overall characteristics of the plasma. When the pedestal density is fixed, density peaking increases fusion power, energy confinement and bootstrap current. On the other hand, peaking reduces the neoclassical tearing mode beta limit [1] and may also lead to impurity accumulation. In a burning plasma only a turbulence-driven particle pinch can result in peaked density profiles because the neo-classical pinch is too weak. The existence of a turbulence-driven particle pinch seems to be proven in L-mode plasmas [2, 3] and it is supported by the theory of turbulence equipartition or thermodiffusion [4]. Its existence in ELMy H-modes is still, however, an open question [2,5,6]. Also from the theory point of view, the situation is not clear as the direction of the turbulence-driven particle flux may depend on other parameters such as the T_e/T_i ratio [4]. Numerical studies on this subject and recent L-mode data are presented in [7].

So far, density peaking studies were motivated mainly by an effort to increase the line-averaged density $\bar{n}$ relative to the Greenwald limit n_{Gr} ($n_{Gr}[10^{20}\,\mathrm{m}^{-3}] = I_p[\mathrm{MA}]/(\pi a[\mathrm{m}]^2)$, I_p is the plasma current and a the minor radius). However, the ratio $\bar{n}/n_{Gr}$ is not an independent dimensionless number and it is correlated with other core dimensionless parameters. One of the strongest correlations is with the core collisionality. Figure 1 illustrates this by plotting the ELMy H-mode JET data in the International Confinement Database. It is seen that plasmas with $\bar{n}/n_{Gr} \approx 1$ have a volume-averaged collisionality more than an order of magnitude larger than the ITER value. Thus, even a weak dependence of the core turbulence on collisionality would mean that the high density plasmas on JET may not represent the core transport expected for ITER. The collisionality dependence of the anomalous transport is not yet clear, in particular, if the same turbulence is responsible for particle and heat fluxes. On the one hand, an increase of trapped electron mode turbulence is predicted towards low collisionalities [8] with anomalous particle pinch as a consequence. On the other hand, a decrease in the core thermal diffusivity with decreasing collisionality is measured in dimensionless scans [9] and is expected from theory due to collisional damping of zonal flows [10].

This paper reports on a new investigation of the density profiles in stationary H-modes under conditions similar to the reference ITER scenario.

2. Experimental conditions

In order to map the dependence of density profiles on collisionality we have scanned collisionality from values corresponding to $\bar{n}/n_{Gr} \approx 1$ down to values as close as possible to ITER. Simultaneously, we restricted ourself to the sawtoothing ELMy H-mode with safety edge factor $q_{95} = 3$–4 and electron and ion temperatures $T_e \approx T_i$. Figure 2 shows the density peaking as a function of the collisionality parameter for selected ELMy H-mode plasmas. The engineering parameters of selected shots from figure 2 are summarized in table 1. The density peaking is characterized by the density difference $\Delta n/\langle n\rangle$. Here, $\Delta n = n_{35} - n_{80}$ and $\langle n\rangle = (n_{35} + n_{80})/2$, where the indices refer to the percentage of normalized poloidal flux coordinate $\sqrt{\psi_N}$. The reason is that it is impossible to characterize the density profile in the gradient zone by a single density scale length and typically the gradient increases with increasing radius. The difference $\Delta n/\langle n\rangle$ is taken across the zone that is not affected by sawteeth and ELMs. The zone bounded by normalized poloidal flux co-ordinates $\sqrt{\psi_N} = 0.35$–0.8 corresponds to normalized toroidal flux co-ordinates of $\rho = 0.3$–0.7 and

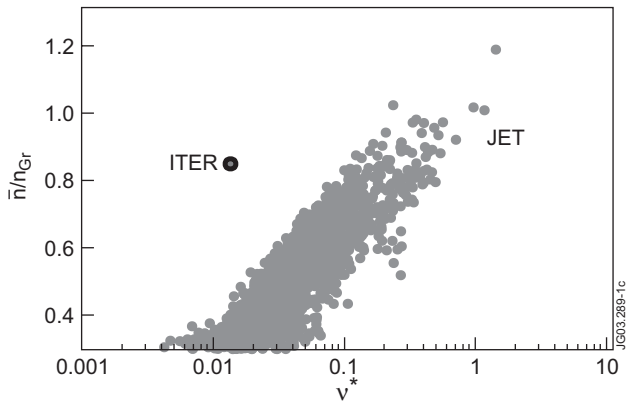

Figure 1. Correlation between density normalized to the Greenwald density and volume averaged collisionality ν^* for JET data in the international ELMy H-mode confinement database DB3V8. $\nu^* = \text{const} \times (R/a)^{1.5} q_{\text{cyl}} R_{\text{geo}} \bar{n}/\langle T \rangle^2$, q_{cyl} is the cylindrical safety factor, R_{geo} is the major radius, $\langle T \rangle$ is the average temperature from energy content W and volume V: $\langle T \rangle = W/(3\bar{n}V)$. The proportionality constant corresponds to a Coulomb logarithm of 16 and effective charge of 1.5.

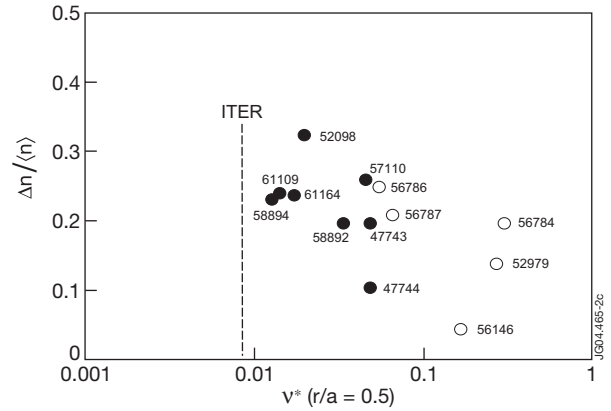

Figure 2. Density peaking $\Delta n/\langle n \rangle$ as a function of collisionality at mid-radius: $\nu^*(r/a = 0.5) = \text{const} \times (R/a/2)^{1.5} q(0.5) R_{\text{geo}} n_{\text{e}}(0.5)/T_{\text{e}}^2(0.5)$. The constant is defined as in figure 1. Full symbols represent plasmas with $P_{\text{RF}} > P_{\text{NBI}}$ while open symbols represent plasmas with $P_{\text{RF}} < P_{\text{NBI}}$. All data are ELMing-sawtoothing with $q_{95} = 3.1$–3.6. The exceptions are JPN47743, JPN47744 and JPN56786 with $q_{95} = 4.1$–4.3.

is shown in figure 3 as vertical lines. In order to reduce the noise level, the LIDAR density profiles are averaged over a period of 1 s.

It is seen from figure 2 that at high collisionality the density peaking data are scattered. On the one hand, flat density profiles are observed, as for example in pulse JPN56146, while with careful balance between gas puffing and beam heating power moderately peaked profiles are also achieved as illustrated by pulse JPN52979 [5]. However, as mentioned above, it is difficult to extrapolate the particle transport characteristics from these high collisionality beam heated plasmas to ITER conditions. Figure 2 also shows the data from medium collisionality plasmas (JPN47743 and JPN47744) previously described in [11]. These type-III ELMy H-modes are part of the scan of increasing RF heating power while the total heating power was held constant. It is seen from figure 2 that in this single scan the plasma with a higher fraction of RF heating (JPN47744) has a flatter density profile than the shots with the same collisionality but lower

Table 1. Engineering parameters of selected shots from figure 2.

JPN	B_T (T)	I_p (MA)	q_{95}	$\bar{n}$ (10^{19} m^{-3})	P_{NBI} (MW)	P_{RF} (MW)
47743	2.7	2.0	4.1	5.5	3.6	7.8
47744	2.7	2.0	4.1	5.5	1.2	10
52098	2.7	2.8	3.3	3.7	2.9	9.5
52979	2.0	1.9	3.1	8.7	10.4	0
56146	2.5	2.7	3.6	10.4	11	3.0
56784	1.7	1.6	3.2	7.4	6.4	0
56786	1.7	1.6	3.2	5.1	9.7	0
56787	1.7	1.2	4.3	3.3	9.6	0
57110	2.7	2.5	3.5	4.6	0	7.2
58892	2.8	2.7	3.3	4.5	3.8	5.9
58894	2.8	2.7	3.2	3.0	3.8	5.0
61109	2.8	2.7	3.2	3.2	3.5	5.9
61164	2.8	2.7	3.2	3.6	3.3	5.9

fraction of RF heating power (e.g. JPN47743). It is important in future to produce more shots with high RF power like JPN47744 to investigate whether the flattening of the density profile seen in this particular scan is systematic.

To access ITER-like collisionality, systematic experiments were performed. To minimize beam fuelling we aimed to replace the beam heating by RF heating as much as possible. For this hydrogen minority heating at fundamental harmonic ICRF (42 MHz) was used (plasma current $I_p = 2.8$ MA, toroidal field $B_T = 2.7$ T, major and minor radii $R_{geo} = 2.89$ m, $a = 0.95$ m). The RF power, $P_{RF} = 5.0$–5.9 MW, is higher than the beam heating power $P_{NBI} = 3.5$–3.8 MW (JPN58894, JPN61164 in table 1). TRANSP calculation shows that the fast ion population is dominated by RF heated hydrogen minority ions (the fraction of fast beam ions is $\sim$2% that at mid-radius). The relative concentration of minority ions is less than 10% and because of the antenna configuration they do not carry parallel current. Therefore, it is not expected that particle transport is significantly affected by fast ions either directly by reducing the number of thermal particles or via friction with thermal particles. At mid-radius, the calculated electron-to-ion heat flux ratio is $\sim$0.7. The ion and electron temperatures are almost equal for this plasma with values $T_e \approx T_i \approx 4$ keV at $\rho = 0.5$. Figure 3 shows the density profile for such a plasma.

The effective charge is measured from carbon charge exchange and for the plasma in figure 3 at mid-radius $Z_{eff}(C) \approx 1.7$. In these RF heated plasmas nickel is expected to be a dominant high-Z impurity. However, the chord-averaged relative concentration of NiXXVI is found to be too low, $(1.5$–$3) \times 10^{-4}$, to contribute significantly to Z_{eff}. Thus, the correction to collisionality in figure 2 from the effective charge is not large and the plasma of JPN58894 represents the collisionality approximately 1.5$\times$ higher than in the ITER nominal plasma ($I_p = 15$ MA, $B_T = 5.3$ T, $q_{95} = 3.0$, $R_{geo} = 6.2$ m, $a = 2.0$ m, $\bar{n} = 10^{20}$ m^{-3}, $Z_{eff} = 1.66$ [12]). As discussed above, reduction of collisionality to ITER values is possible only at the expense of lower normalized density. For JPN58894, the value is $\bar{n}/n_{Gr} \approx 0.29$, consistent with the dataset in figure 1.

The plasmas of shot JPN58894, and those in its neighbourhood are sawtoothing and typically $m = 3$, $n = 2$ neoclassical tearing modes are excited at the beginning of the flat-top of ICRH power. In order to minimize the possible effect of the tearing mode on particle transport we have repeated the JPN58894 with modified RF heating, with the aim of reducing the sawtooth amplitude [13]. A slower ICRF power ramp and shifting the resonance

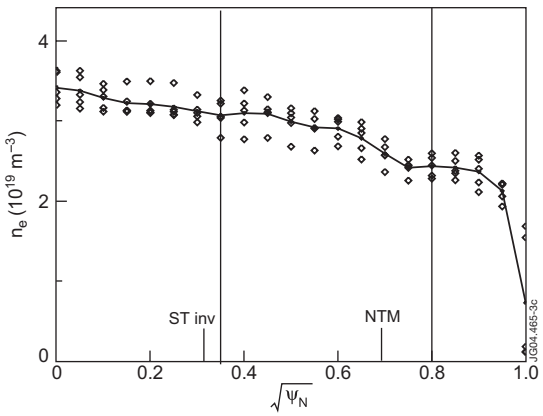

Figure 3. Density profile for shot number 58894. The diamonds are the instant LIDAR data mapped to poloidal flux at multiple time points between $t = 62.7$ and 63.9 s. The solid line is the averaged density profile over this interval. Approximate positions of the sawtooth inversion radius and the $m = 3$, $n = 2$ neoclassical tearing mode (NTM) are shown.

from the magnetic axis to the inner $q = 1$ surface for 50% of the heating power resulted in a reproducible suppression of the $m = 3, n = 2$ neoclassical tearing mode. The sawtooth period during the RF flat-top phase, however, was not changed significantly and thus the question of which of these two actions improved tearing mode stability remains open. The effect of suppression of the neoclassical tearing mode on the global density peaking parameter $\Delta n/\langle n\rangle$ is found to be small. This is seen from figure 2 where the data from shots without the $m = 3$, $n = 2$ neoclassical tearing mode (JPN61109, JPN61164) have density peaking similar to the plasma JPN58894 in which the mode was present. Suppression of the neoclassical tearing mode, however, resulted in increase of normalized beta from $\beta_N \approx 0.8$ to 1.0.

Plasmas represented by the shot in figure 3 are in type-III ELMy regimes. This is an unwanted consequence of the attempt to maximize the fraction of RF heating power, which is only possible at low total power below transition to the type-I ELMy regime. The relatively low level of RF power is also the reason why the additional neutral beam heating is used to enter the H-mode regime but this power was deliberately kept low to minimize particle source. The absence of type-I ELMy plasmas with RF-only heating at low collisionalities still leaves room for a possible correlation between the density peaking and the plasma edge. Such a correlation between ELM character and density peaking could be explained only if ELMs generate global transport events affecting the particle transport at mid-radius. Such an effect, however, was not reported for type-III ELMs. Another possible correlation could come from the stiffness of temperature profiles. A lower pedestal temperature in type-III ELMy H-mode could mean a higher level of turbulence in the confinement region than in the type-I ELMy regime. This, in turn, could enhance the turbulence driven pinch with respect to its level in the type-I regime. Note, however, that such an effect would require that the anomalous diffusivity and pinch velocity have different dependences on the turbulence amplitude.

In summary, it is seen from figure 2 that the group of plasmas described above has reached a collisionality (Z_{eff} corrected) approximately 1.5× the value for the reference ITER ELMy H-mode scenario. At low collisionalities, only peaked density profiles are observed in contrast to high collisionality cases. The density peaking, however, is relatively modest. The question of whether this is evidence for anomalous particle pinch or if it is the result of particle sources is addressed later.

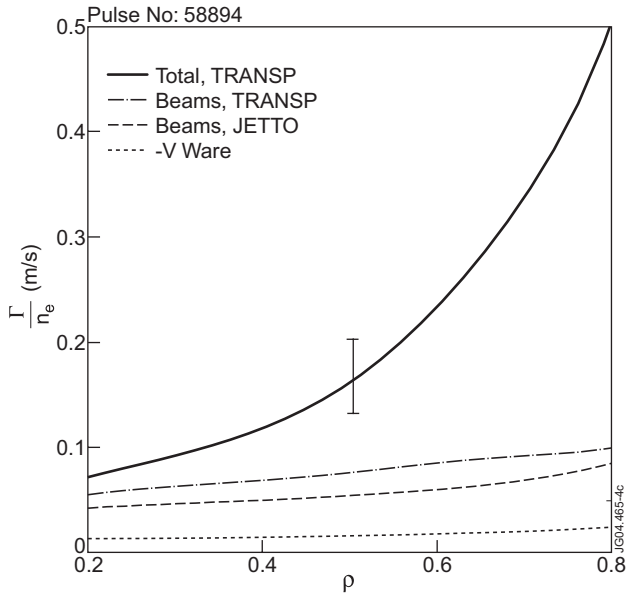

Figure 4. Calculated normalized particle fluxes for JPN58894 at 62.5–63.5 s. Ware pinch velocity ($-V_W$) is shown for comparison. The error bar $\pm 0.03\,\mathrm{m\,s^{-1}}$ represents the uncertainty due to edge ion temperature measurement (see table 2).

3. Particle flux

The existence of an inward particle pinch should be ideally demonstrated in a plasma with zero particle flux. Inward pinch is then manifested as a peaked density profile. As mentioned earlier, such conditions are difficult to achieve and the particle flux is not negligible. The electron flux density through the magnetic flux surface is the sum of two terms: a contribution from the neutral beam (including halo) and a contribution from neutrals penetrating from the gas puffing and the wall:

$$\Gamma = \Gamma_{\mathrm{Beam}} + \Gamma_{\mathrm{Wall}} = \frac{S_{\mathrm{Beam}} + S_{\mathrm{Wall}}}{\Sigma}.$$

Here, S_{Beam} and S_{Wall} are the electron sources inside the given magnetic flux surface and Σ is the flux surface area [14]. The contribution from neutrals produced by radiative recombination of the main ions is small in our case due to the high temperature and low density. In principle, there is also a contribution from the temporal changes in electron density but, for our stationary conditions, this term is small. For JPN58894 at $t = 63$ s the flux at mid-radius is equivalent to $\Gamma/n_{\mathrm{e}}|_{\rho=0.5} \approx -(a/4)(\mathrm{d}\bar{n}/\mathrm{d}t)/\bar{n} = 1.6\,\mathrm{cm\,s^{-1}}$, where n_{e} is the local electron density.

Figure 4 shows the normalized electron flux density through the particular magnetic flux surface. The figure shows the total flux and the flux due to the neutral beams. The difference between these two terms is the flux caused by neutrals penetrating from the gas puffing and the wall.

The particle flux due to the neutral beams is calculated using the TRANSP code by the Monte Carlo method and using the JETTO/PENCIL code. It is seen from figure 4 that the fluxes given by these two codes are in relatively good agreement and the out-flux at mid-radius

($r/a = 0.5$) is equivalent to

$$\frac{\Gamma_{\text{Beam}}}{n_{\text{e}}} = 0.074\,\text{m}\,\text{s}^{-1}.$$

Note that the TRANSP calculation includes the charge exchange halo neutrals while in JETTO/PENCIL these are not included. To a first approximation, Γ_{Beam} is proportional to the beam heating power and, thus, the value $\Gamma_{\text{Beam}}/n_{\text{e}}$ above is ~2.3–2.7 smaller than it would be if all the heating power were to be provided by beams (table 1, JPN58894, JPN61109).

The second contribution to the outward particle flux is due to the edge neutrals penetrating into the core region. This inward particle flux of neutrals is calculated by the 1.5-D FRANTIC code [15–17] implemented into TRANSP. FRANTIC performs neutral gas transport calculation for tokamak core plasmas, taking into account charge exchange and impact ionization atomic reactions in a simplified nested cylindrical flux surface geometry. The boundary conditions for the FRANTIC code in TRANSP use the experimental gas valve rate with efficiency 1 for neutrals entering the separatrix and the integrated D_α photon flux (scaled up by 10 to convert from photons to the ionization rate within the separatrix). For our conditions, the calculated flux at mid-radius due to wall and gas puff neutrals is equivalent to $\Gamma_{\text{Wall}}/n_{\text{e}} = 0.093\,\text{m}\,\text{s}^{-1}$, i.e. approximately equal to the particle flux due to the neutral beam (figure 4).

The fact that neutrals from the wall may play a role in the particle balance at mid-radius has been reported on TFTR [18]; however, it is still somewhat surprising for large plasmas as on JET. Therefore, this result has been checked by the stand-alone FRANTIC code. Stand-alone FRANTIC is the same code as used in TRANSP but allows more flexible sensitivity study of the results on boundary conditions. It also allows us to include the edge density profile from Li-beam diagnostics, in addition to the core LIDAR data, so that a more accurate density profile is used in calculations, particularly in the sensitive edge region. For these studies we used FRANTIC in a mode when beam halo and beam ionization source are not included. Thus, the calculated flux is comparable to Γ_{Wall} from TRANSP, with small differences due to the effect of fast ions on the ionization profile of wall neutrals and the beam contribution to the D_α photon flux.

Stand-alone FRANTIC provides the full radial profile of D_α emission (including the region outside the separatrix) and thus allows us to improve the boundary conditions for wall and gas puff neutrals. Because the region outside the separatrix contributes significantly to the D_α emission, this is one of the main improvements in comparison with FRANTIC embedded in TRANSP, which is concerned only with the region $r/a < 1$ and uses 'effective' boundary conditions at $r/a = 1$ (see above). The stand-alone FRANTIC calculates the neutral atom density in two steps. In the first step, the relative neutral density is obtained in the whole region where the electron density profile is given. In our case, the range is $r/a = 0$–1.06, where $r/a = \sqrt{A/\pi}$, A being the cross-sectional area inside the flux surface taken from equilibrium reconstruction and $r/a > 1$ is extrapolation. In the second step, the relative neutral density profile is multiplied by a single constant to obtain the absolute neutral atom density $n_0(r/a)$. The multiplier is adjusted in such a way that the calculated total D_α photon flux corresponds to the measured one.

The results of calculations using the stand-alone FRANTIC code are summarized in table 2. Row 2 shows the result when the calculated total D_α photon flux matches the measured flux from the whole plasma (2.6×10^{21} photons s^{-1}), including the divertor. As a result, the neutral atom density outside the plasma is found to be $n_0(r/a = 1.06) = 4.7 \times 10^{16}\,\text{m}^{-3}$. With this setting, the stand-alone FRANTIC gives a normalized flux velocity at the mid-radius of $\Gamma_{\text{Wall}}/n_{\text{e}} = 0.10\,\text{m}\,\text{s}^{-1}$. This value agrees to within 10% with calculations given by FRANTIC embedded inside TRANSP (row 1 of table 2). The reason is that the different

Table 2. Electron flux due to wall and gas puff neutrals for different boundary conditions. JPN58894, $t = 62.5$–63.5 s. E_0 is the energy of wall neutrals. R is the reflection coefficient of charge exchange neutrals from the wall. Row 1 is for FRANTIC embedded in TRANSP while rows 2–6 are for stand-alone FRANTIC.

	Boundary conditions				Calculated values	
	Neutral influx	E_0 (eV)	R (%)	T_i $r/a = 0.95$ (keV)	n_0 $r/a = 0.95$ (10^{15} m^{-3})	Γ_{Wall}/n_e $r/a = 0.5$ (m s^{-1})[a]
1	From gas valve rate and estimate of edge ionization rate as $10 \times D_\alpha$ photons	3–10	30	1.0	1.1	0.093
2	By matching calculated and measured total D_α emission	5	90	1.0	1.0	0.10
3	Same as 2	0.55	90	1.0	0.45	0.038
4	Same as 2	5	90	0.7	1.0	0.075
5	Same as 2	5	90	1.3	1.0	0.12
6	Same as 2 but excluding D_α emission from divertor	5	90	1.0	0.072	0.0077

[a]Note that total flux is $\Gamma = \Gamma_{Beam} + \Gamma_{Wall}$ with $\Gamma_{Beam}/n_e = 0.074\,\mathrm{m\,s^{-1}}$ at $r/a = 0.5$.

boundary conditions at the separatrix in both cases effectively gives similar neutral density at $r/a = 0.95$. At this point and deeper into the core all neutrals exist only as 'thermal', i.e. they are all the result of charge exchange processes and their profile is given only by the main plasma parameters.

To understand further how the rather small number of neutrals that are present in the core of the JET plasmas may generate significant particle flux we can calculate the influx of neutrals at the mid-radius. When the mean free path of charge exchange is shorter than the density and temperature gradients the kinetic theory for neutral flux gives [19]:

$$\Gamma_0 = n_0 \lambda_{cx} \sqrt{\frac{T_0}{m_i}} \left(-\frac{\nabla n_0}{n_0} - 0.76 \frac{\nabla T_0}{T_0} \right). \tag{1}$$

This equation is equation (27′) of [19] and the mean free path of charge exchange is $\lambda_{cx} = (2.93 \sigma_{cx} n_i)^{-1}$, as given by equation (24) of [19]. In addition to the short mean free path approximation, equation (1) is derived using the Chapman–Enskog method in order to calculate transport coefficients from kinetic equations. At $\rho = 0.5$, the calculated neutral density by FRANTIC is $n_0 = 2.0 \times 10^{13}\,\mathrm{m^{-3}}$ with $n_0/\nabla n_0 = 0.22\,\mathrm{m}$. The temperature of neutrals is close to the ion temperature $T_0 \approx T_i = 4\,\mathrm{keV}$ with a scale length of $T_0/\nabla T_0 = -0.76\,\mathrm{m}$ ($T_i/\nabla T_i \approx -0.8\,\mathrm{m}$). At this temperature and ion density $n_i = 3 \times 10^{19}\,\mathrm{m^{-3}}$ the charge exchange mean free path is $\lambda_{cx} = (2.93 \sigma_{cx} n_i)^{-1} = 0.098\,\mathrm{m}$ ($\sigma_{cx} = 1.1 \times 10^{-19}\,\mathrm{m^2}$ [20]) so that the ordering $\lambda_{cx} \ll n_0/\nabla n_0, T_0/\nabla T_0$ is satisfied, though marginally for $n_0/\nabla n_0$. In the steady state the neutral influx in the closed volume has to be balanced by the outward electron flux calculated from the ionization source:

$$\Gamma(r) = r^{-1} \int_0^r S r' \,\mathrm{d}r', \tag{2}$$

where S is the ionization source calculated by FRANTIC. Figure 5 shows that the fluxes given by equations (1) and (2) are indeed in a good agreement. This agreement is not trivial as the neutral transport in FRANTIC is calculated by a method different from kinetic theory [19]. Note that while FRANTIC calculates the neutral density and ionization source the kinetic theory given by equation (1) is the local theory of neutral transport and is not concerned with ionization. The agreement between these fluxes confirms the consistency of the numerical

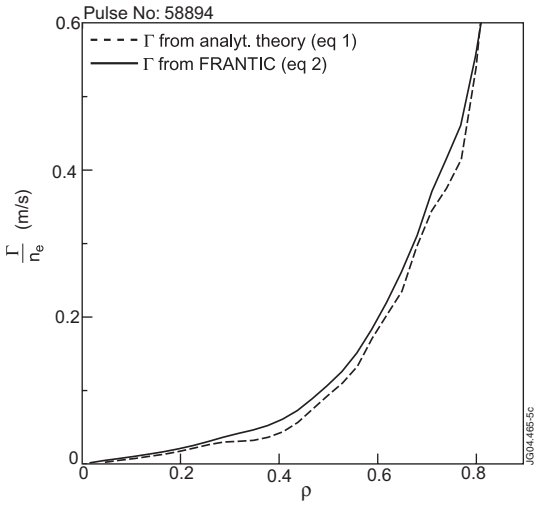

Figure 5. Comparison of the normalized flux from analytical theory with the flux calculated by FRANTIC from the ionization source. The conditions are the same as in table 2, row 2.

procedure in FRANTIC and the validity of the approximation used in the analytical theory [19] for our conditions.

The above stand-alone FRANTIC results have been obtained for energy of edge neutrals $E_0 = 5$ eV. To exhibit the sensitivity of the core neutral density to the choice of energy of edge neutrals we performed further sensitivity studies while other parameters were unchanged. For example, by reducing the energy to $E_0 = 0.55$ eV the neutral density and particle flux drop by a factor of $\sim$2 (see table 2, row 3). Published spectroscopy data [21] suggest that the edge neutrals may be a 50%–50% mixture of particles with energies $E_0 = 0.55$ and 5 eV. For this mixture, electron flux due to wall neutrals would, then, be $\Gamma_{\mathrm{Wall}}/n_{\mathrm{e}} = 0.07\,\mathrm{m\,s^{-1}}$ and the total flux would be 25% smaller than that shown in figure 4. Therefore, we conclude that the uncertainty in the energy of edge neutrals, though significant, does not have a large impact on the calculated particle flux.

The ion temperature at the very edge is set equal to the electron temperature in our calculations. Sensitivity studies show that, with electron temperature and other parameters kept constant, the neutral density at the mid-radius is roughly proportional to the ion temperature in the region $r/a = 0.9$–1. Table 2, rows 4 and 5 illustrate this when the edge ion temperature is varied within the experimental scatter of charge exchange measurement. The measured ion temperature at the edge varies within $T_{\mathrm{i}}(r/a = 0.95) = 1.0 \pm 0.3$ keV for JPN58894 during the time interval $t = 62.5$–63.5 s.

The largest uncertainty in the calculation of neutral particle flux comes from the poloidal asymmetry of the D_α emission. In the above calculations, all the emission (main chamber plus divertor) has been included in the 1.5-D FRANTIC modelling. However, because of the low level of gas puff most of this emission ($\sim$90%) originates in the divertor region. Due to the complex geometry of the divertor, the choice with all D_α emission included represents the upper limit for the particle flux. When the D_α emission from the divertor is completely excluded the flux becomes negligible (see table 2, row 6). Somewhat indirect checks of how much of the divertor emission has to be included can be made by calculating the effective electron diffusivity just inside the separatrix. If all D_α emission from the divertor is included, then, the average effective diffusivity (assuming no pinch) between the separatrix and the top of

the pedestal ($r/a = 0.95$–1) is found to be $D_{\mathrm{e,eff}} \approx 0.8\,\mathrm{m^2\,s^{-1}}$ (for case no. 2 in table 2). If the whole divertor region is excluded, this value would be reduced tenfold: $D_{\mathrm{e,eff}} \approx 0.08\,\mathrm{m^2\,s^{-1}}$ (for case no. 6 in table 2). Such a value seems to be very low for the region dominated by ELMs. This could be an indication that most of the divertor D_α emission has to be taken into account when calculating the neutral source in the core. Note that the electron flux in the core due to wall neutrals is only a fraction ($\leqslant \frac{1}{2}$) of the total flux and, therefore, a factor of 10 difference in the edge diffusivity translates only to a factor of $\sim$2 uncertainty in the particle diffusivity in the core.

The uncertainty of how much of the divertor neutrals contribute to the particle source in the plasma can be answered only by detailed two-dimensional modelling of the neutral distribution. In this context, we refer to the recent detailed study in [22] using the EDGE2D code, which analyses the ELMy H-mode plasmas with NBI heating and densities somewhat higher than that in our case, from figure 4. In this study, the neutral density in the core is found to be lower than in our case and, consequently, the particle flux is given only by neutral beams. When FRANTIC and EDGE2D codes are run for the case in [22] so that they match the D_α emission in the main chamber (excluding divertor region) the calculated neutral densities agree within 30%. Therefore, as expected, the problem is reduced to modelling of neutrals in a region around the X-point. 1.5D-modelling inevitably underestimates the flux expansion in the divertor area, which can result in overestimation of the neutral flux from the divertor. From the other side, the lower penetration of neutrals from the divertor to the core calculated by EDGE2D may be a consequence of low ion temperature at the separatrix around the X-point in EDGE2D. A consequence of such a temperature drop is an extremely large electron density gradient across the separatrix around the X-point, indicating very low turbulence in this region. It is, therefore, possible that the influx of neutrals from the divertor is linked to the level of the plasma particle transport around the X-point. It is, however, outside the scope of this paper to quantify such a relationship. The toroidal modulation of neutrals should be moderated by the fact that the gas is puffed via toroidal rings. Other sources of toroidal modulations could be the wall recycling and beam locations; however, these uncertainties are believed to be smaller in comparison with the factor of 10 from the poloidal modulation discussed above.

Up to this point we conclude that we have designed the H-mode plasma that matches the ITER collisionality and simultaneously minimizes the electron particle flux. At the mid-radius ($r/a = 0.5$), the flux is in the range

$$\frac{\Gamma}{n_\mathrm{e}} = 0.07\text{–}0.2\,\mathrm{m\,s^{-1}}.$$

The uncertainty is due to wall neutrals where almost all the flux comes from the divertor region. The lower limit ($0.07\,\mathrm{m\,s^{-1}}$) represents the flux from neutral beams only and the upper limit ($0.2\,\mathrm{m\,s^{-1}}$) the flux when all wall neutrals are included. It has to be noted that the significant flux due to the wall neutrals is a property of low collisionality (lower density) plasmas and as such is not typical for JET and unlikely for ITER. This case has been chosen deliberately to create collisionality conditions that are as close as possible to the ITER nominal plasma. This complication again underlines the importance of a case-by-case analysis of particle sources before statements about the character of particle transport are made.

The electron flux Γ/n_e is still relatively large when compared to the value expected in ITER. In the ITER reference scenario, the flux due to 33 MW of neutral beam with energy of 1 MeV [12] corresponds at mid-radius to $\Gamma/n_\mathrm{e} \approx 0.007\,\mathrm{m\,s^{-1}}$. The particle source due to the wall neutrals will be localized at the edge where particle transport was suggested to be neoclassical [23, 24, 12] and will not contribute to the flux in the turbulent core area. Therefore, we stress again that the relatively large particle flux in the core in our JET plasmas do not

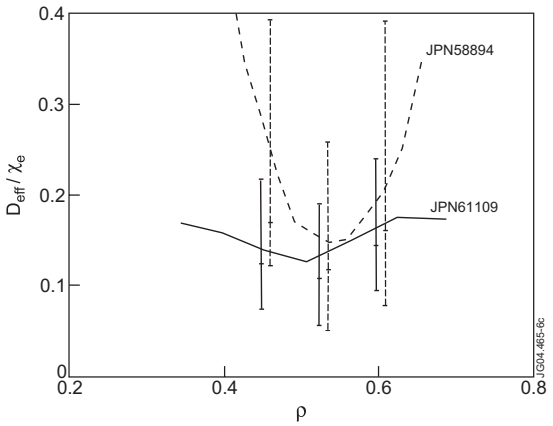

Figure 6. The ratio of effective particle and electron heat diffusivities as calculated by TRANSP. The values are averaged over 62.5–63.5 s. The error bars represent the spread of values calculated at five individual time slices of LIDAR measurements during this time interval. Calculations are with all neutrals from the divertor included. The extended error bars towards the lower values indicate the uncertainty if all divertor flux is excluded.

represent the situation expected in ITER but is an unavoidable consequence of the attempt to match the ITER core collisionality in H-mode.

4. Pinch velocity

Conventionally, the particle velocity, V, is defined from the equation:

$$\frac{\Gamma}{n_e} = -D_e \frac{\nabla n_e}{n_e} + V, \tag{3}$$

where ∇n_e is the electron density gradient and D_e the electron diffusivity. It should be noted that such a linear dependence already assumes that the turbulence driving the particle flux does not depend on the density gradient itself. In the practically important case with $\Gamma > 0$ the solution of equation (3) is ambiguous and the inferred value of pinch velocity depends on the assumption on D_e. In the case when transport is dominated by turbulence basic theoretical considerations predict that the particle diffusivity is linked to heat diffusivity. For the case in figure 4 the condition for turbulence driven transport is well satisfied because electron and ion heat diffusivities at mid-radius are $\chi_e \approx 0.5\chi_i \approx 1\,m^2\,s^{-1}$ while the ion neoclassical heat diffusivity is $\chi_{i\,NC} \approx 0.05\,m^2\,s^{-1}$. The quantitative relationship between particle and heat diffusivities is not well known. For electrostatic turbulence, the random walk argument provides the ratio $D_e/\chi_e = 2/3$. In order to quantify this ratio more accurately non-linear simulations using the model described in [4] were performed. These calculations provide the ratio $D_e/\chi_e \approx 0.3$–0.4, and this value is approximately constant across the gradient zone. Simulations were done with a deliberately large central particle source so that the correction to the particle flux from pinch is small and $D_e \approx -\Gamma/\nabla n_e$.

Figure 6 shows the ratio of particle to heat diffusivities D_{eff}/χ_e if no anomalous pinch is assumed ($D_{eff} = D_e(V = V_W)$, where $V_W \approx 0.02\,m\,s^{-1}$ is the Ware pinch velocity). It is seen that the ratio has a minimum of $D_{eff}/\chi_e = 0.15$–0.2 in the region between $\rho \approx 0.5$–0.7. Note that without the contribution of wall neutrals this minimum would be even lower ($D_e/\chi_e \approx 0.1$) as indicated by extended error bars in figure 6. The region of low diffusivity coincides with

the zone of the steeper density gradient where the time-averaged density scale-length drops to $L_n \approx 1$ m. The zone of low D_{eff}/χ_e extends deeper into the centre for the plasma without the $m = 3/n = 2$ neoclassical tearing mode (JPN61109) in comparison with plasma with such a mode (JPN58894). This may be an effect of the mode on anomalous transport although this has not been studied in detail. This important aspect of particle transport deserves further attention.

The minimum of D_{eff}/χ_e is lower than the value predicted by available theories. However, whether this discrepancy actually reflects the existence of anomalous pinch is impossible to determine because the particle flux in our case is still not zero. We can only speculate that if the dependence of the particle flux on the density gradient is linear (equation (3)) with the diffusivities ratio, say $D_e/\chi_e = 0.3$, then, the inferred anomalous pinch velocity will be $V \approx -(0.1\text{–}0.2)\,\mathrm{m\,s^{-1}}$ or $-V/D_e \approx 0.4\,\mathrm{m^{-1}}$ at $\rho \approx 0.6$. Assuming the higher ratio, $D_e/\chi_e \sim 1$, would result in a particle pinch of $-V/D_e(\rho \approx 0.6) \approx 0.8\,\mathrm{m^{-1}}$. On the other hand, if $D_e/\chi_e = 0.17$, then, no anomalous particle pinch is inferred, $V = 0$. Note again, that it is the regime with very low particle flux we need to extrapolate because in the ITER the normalized flux, Γ/n_e, is smaller than in our JET case. This is, in addition to the low beam source, because the particle source from gas puffing in ITER will be localized at the edge and not in the region of turbulent transport.

Finally, let us compare our results with particle transport models used in ITER simulations in the core. Typically, the normalized diffusivity ranges from $D_e/\chi_e = 0.1(1 + \chi_i/\chi_e)$ [23] to $D_e/\chi_e = 1$ [24] and the anomalous pinch is set to zero. An anomalous pinch of up to $-V/D_e \approx 0.4\,\mathrm{m^{-1}}$ with $D_e/\chi_e = 1$ is considered in [25]. It is seen that the calculated values of D_{eff}/χ_e presented in this paper include the lower end of values typically used in ITER simulations. This fact is independent of interpretation (with or without anomalous pinch).

To discuss the quantitative consequences of different particle transport models for ITER performance one has to perform transport analyses similar to the one in [24]; however, such a study is outside the scope of this paper. Nevertheless, some effects can be envisaged. If weak pinch is present it will enhance fusion performance due to peaked density profiles. This has been shown in [25] where the pinch $-V/D_e \approx 0.4\,\mathrm{m^{-1}}$ is introduced, while keeping the diffusivity $D_e/\chi_e = 1$. As a result, the density profile peaks up to $\Delta n/n \sim 0.3$. The fusion power increases somewhat less, by 20%, due to increased helium peaking. When the lower values of particle diffusivity, $D_e/\chi_e = 0.1(1 + \chi_i/\chi_e)$, and no anomalous pinch are used, combined with a fuelling beam, then, the density profiles are modestly peaked and the fusion gain is $Q = 15$ [23]. Finally, note that the core particle transport also affects the fuelling by pellets as they deliver particles at the outer part of the plasma. In particular, the low values of particle diffusivities may change the requirements for pellet injection so that the ELM mitigation and fuelling may require separate systems.

5. Conclusion

Dedicated experiments have been performed in JET to produce ELMy H-mode plasmas with ITER-like collisionality, significant RF heating, $T_e/T_i \approx 1$ and $q_{95} \approx 3$. Modestly peaked density profiles are found under these conditions. Particle balance shows that the outward flux at mid-radius is still significant in these plasmas and thus uncertainty in the determination of the anomalous pinch velocity remains large. It is found that at low collisionality the error bars of the ratio of particle-to-thermal diffusivities comprises the area where $D_{e,eff}/\chi_e \sim 0.2$ if no anomalous pinch is assumed. Low values of particle diffusivities can be interpreted as an indication for an anomalous pinch if the particle flux depends linearly on the density gradient, and the particle diffusivity D_e is sufficiently large. The uncertainties justify further studies

aiming to improve the particle transport model under ITER relevant conditions. Further work is needed to expand the database, in particular towards high RF power and relevant collisionality. Experiments are envisaged on JET using a new RF antenna that should deliver higher power and be capable of operation with type-I ELMs. Higher RF power should increase plasma temperature and thus reduce collisionality further. In addition, it may allow operation in the type-I ELMy regime with RF heating only and thus remove the uncertainty due to the possible link between the pedestal temperature and turbulence in the core. Simultaneously, this will reduce the particle flux to levels given by wall neutrals only. As for the flux due to wall neutrals, improved modelling is required to address the large uncertainty. Operation at somewhat higher densities should decrease the flux of wall neutrals. This could be possible without significant departure from low collisionalities if higher heating power is available.

Acknowledgments

This work has been conducted under the European Fusion Development Agreement and was funded partly by the United Kingdom Engineering and Physical Sciences Research Council and by EURATOM. RB was supported by US DOE contract DE-AC02-76CH)3073. OS and HW were also supported by the Swiss National Science Foundation. Discussions with Dr P Helander about particle transport and the help of Dr D Howell regarding sawteeth and tearing mode localization are gratefully acknowledged. The authors thank Dr McCune for help with the TRANSP code and Dr Weisen for help during the experiments.

References

[1] Günter S *et al* 2004 *Nucl. Fusion* **44** 524–32
[2] Garzotti L *et al* 2003 *Nucl. Fusion* **43** 1829–36
[3] Weisen H and Minardi E 2001 *Europhys. Lett.* **56** 542
[4] Garbet X *et al* 2003 *Phys. Rev. Lett.* **91** 035001
[5] Valovič M *et al* 2002 *Plasma Phys. Control. Fusion* **44** 1911
[6] Stober J *et al* 2001 *Nucl. Fusion* **41** 1535
[7] Garbet X *et al* 2003 *30th EPS Conf. on Controlled Fusion and Plasma Physics (St Petersburg, 2003)* vol 27A (ECA) P-2.87
[8] Angioni C *et al* 2003 *Phys. Rev. Lett.* **90** 20503
[9] Petty C C *et al* 1999 *Phys. Plasmas* **6** 909
[10] Lin Z, Hahm T S, Lee W W, Tang W M and Diamond P H 1999 *Phys. Rev. Lett.* **83** 3645
[11] Rimini F G, Saibene G and the JET team 2002 *Nucl. Fusion* **42** 86
[12] *ITER Final Design Report* chapter 4, p 8, http://www.iter.org/ITERPublic/ITER/PDD4.pdf
[13] Sauter O *et al* 2002 *Phys. Rev. Lett.* **88** 105001
[14] McCune D. In TRANSP the corresponding variables are $S_{\mathrm{Beam}} = \mathrm{SBE} + \mathrm{SCEV}$ and $S_{\mathrm{Wall}} = \mathrm{SCEW}$, TRANSP code, http://w3.pppl.gov/transp
[15] Tamor S *SAI Report* 023-79-1056LJ
[16] Korotkov A A and Zinov'ev A N 1989 *Sov. J. Plasma Phys.* **15** 136
[17] Tunklev M *et al* 1999 *Plasma Phys. Control. Fusion* **41** 985
[18] Budny R *et al* 1990 *J. Nucl. Mater.* **176 & 177** 427–31
[19] Helander P, Krasheninikov S I and Cato P J 1994 *Phys. Plasmas* **1** 3174
[20] Janev R K and Smith J J 1993 *Nucl. Fusion* **4** (Suppl.) 79
[21] Mertens Ph *et al* 2001 *Plasma Phys. Control. Fusion* **43** A349
[22] Kallenbach A 2004 *Plasma Phys. Control. Fusion* **46** 431
[23] Pacher G W *et al* 2004 *Plasma Phys. Control. Fusion* **46** A257–64
[24] Polevoi A R *et al* 2003 *Nucl. Fusion* **43** 1072
[25] *ITER Final Design Report* chapter 4, p 15, http://www.iter.org/ITERPublic/ITER/PDD4.pdf